Mario Nascimento, 2025, 13:3
ISSN (Online): 2348-4098
ISSN (Print): 2395-4752

International Journal of Science, Engineering and Technology

An Open Access Journal

Medium-Free Local Determination of Earth's Gravitational Field: A Multi-Modal Laboratory Study across Quantum, Classical, and Relativistic Regimes

Mario Nascimento, Joao Silva, Mariana Alves
Advanced Mind Research Institute (AMRI)

Abstract- We determine the local gravitational acceleration and potential with three indepen- dent ultra-high-vacuum (UHV) instruments: (i) a dual-species 87Rb / 39K Mach–Zehnder atom interferometer, (ii) laser-tracked free-fall of centimetre spheres whose bulk den- sities differ by a factor eight, and (iii) a vertically separated pair of 87Sr optical-lattice clocks. All experiments operate below 10^{-5} Pa, where hydrostatic forces are < 10^{-11} of the test weight. The three sensors yield g = 9.803 07 ± 0.000 07 m s^{-2} (atom interferom- eter, Rb), g = 9.803 02 ± 0.000 29 m s (free fall), and g = 9.804 ± 0.0017 m s (optical clocks), in mutual agreement at the 3 × 10 level. A pressure-variation study up to 10^{-1} Pa shows no discernible change in g ($\partial g/\partial p = -0.8 \pm 1.7 \times 10^{-5}$ m s^{-2} Pa^{-1}). The fractional differential acceleration between the two atomic species is η < 7.6×10 (95% C.L.), confirming the composition independence of free fall. Because the quantum phase (interferometer) and fractional frequency shift (clocks) cannot be generated by hydrostatic pressure, and the classical drop occurs where such pressure is negligible, the data establish gravity—not density sorting or buoyancy—as the unique driver of weight and free fall.

Keywords- gravimetry, atom interferometry, optical clocks, general relativity, ultra-high vacuum, equivalence principle, quantum sensors

I. INTRODUCTION

High-accuracy gravimetry [Torge & Mu¨ller, 2001, Rosi et al., 2014] underpins geodesy, navi- gation, and tests of fundamental physics. While Newtonian mechanics attributes falling mo- tion to universal gravitational attraction, alternative heuristics sometimes invoke **relative- density** or buoyant forces as if they were primary causes. A decisive assessment therefore requires: (1) measurements in media where hydrostatic forces are a priori negligible; (2) at least one observable that cannot emerge from contact forces; and (3) direct quantification of any residual density dependence. We satisfy these criteria simultaneously with three UHV instruments that span quantum, classical and relativistic regimes (Table 1).

Table 1: Key parameters of the three gravimeters used in this study.

Sensor	Operating principle	Pressure / Pa	Single-shot g prec. / ppm
Dual-species atom interferometer	Raman phase $k_{eff} g T^2$	9×10^{-10}	8 (Rb) / 11 (K)
Laser-tracked free fall	Quadratic fit $z(t)$	1×10^{-6}	30
Optical-lattice clocks	GR redshift $g\Delta h/c^2$	3×10^{-8}	170

II. GRAVITATIONAL, BUOYANT, AND DRAG FORCES IN VACUUM

Hydrostatic equilibrium demands $\nabla P = -\rho f\ g$. Integrating over the submerged volume V gives Fb = ρf V g. If ρf → 0 or g → 0 then Fb → 0; buoyancy is therefore a derived force that cannot exist without an antecedent gravitational field.

2. Residual hydrostatic force in UHV

At p = 10^{-5} Pa and T = 293 K, the ideal-gas number density is n ≃ 2.5 × 10^{17} m^{-3}, giving mass density ρ_f = nm_{air} ≈ 4 × 10^{-8} kg m^{-3}. For a 20-mm steel sphere (V = 4.2 × 10^{-5} m^3), F_b < 4 × 10^{-11} N = 4 × 10^{-12} mg, below the noise floor of the drop experiment by five orders of magnitude

3. Free-Molecular Drag

The drag deceleration in the molecular-flow regime is $a_d = (3\rho_f v \bar{v})/(4R\rho_s)$ [Achenbach, 1973]. With v = 2 m s^{-1}, mean thermal velocity $\bar{v}$ = 480 m s^{-1}, and ρ_s = 7.8 g cm^{-3}, a_d < 2 × 10^{-9} g.

III. THEORY OF THE THREE SENSORS

Atom Interferometer: Three-pulse sequence π/2–π–π/2 with interrogation time T gives

$$\Delta\varphi = k_{\text{eff}} g T^2 + \varphi_{\text{vib}} + \varphi_{\text{AC}}, \tag{1}$$

where k_{eff} = 4π/λ is 16.10 μm^{-1} for 87Rb (λ = 780 nm). Vibration phase φ_{vib} is cancelled by common-mode readout of the retro-mirror with a seismometer; AC-Stark shift φ_{AC} is suppressed by k-reversal.

Optical clocks: The proper time along a stationary world-line at height h differs by Δτ = ΔΦ/c^2 τ = gΔh τ /c^2. The fractional frequency offset is

$$\frac{\Delta\nu}{\nu} = \frac{g\,\Delta h}{c^2} = 8.18 \times 10^{-17} \left(\frac{g}{9.803\,\mathrm{m\,s^{-2}}}\right)\left(\frac{\Delta h}{0.750\,\mathrm{m}}\right). \tag{2}$$

IV. EXPERIMENTAL APPARATUS

1. Ultra-High-Vacuum Infrastructure

All three instruments share a 2.5-m-radius clean room with a redundant dry-pump/ion- pump chain. Pressures are monitored by hot-cathode gauges (calibrated at PTB) with 10 % accuracy.

2. Dual-Species Atom Interferometer

A two-dimensional MOT emits a cold beam captured in a 3D mirror-MOT (Fig. 1a). After sub-Doppler cooling to 2 μK the atoms are launched in a fountain. The Raman lasers are phase-locked via an optical frequency comb; common retro-mirror defines vertical k_{eff}.

3. Free-Fall Track

A 2.00±0.01-m stainless tube houses kevlar-suspended voice-coil clamps. A 100-kHz quadrature encoder (532-nm retro-reflected beam) provides timing; synchronisation uses a top-mounted photodiode.

4. Optical-lattice clocks

Two 87Sr fountains (linewidth 1 Hz) are trapped in vertical 1-D optical lattices at the clock magic wavelength 813 nm. A phase-stabilised telecom fibre transfers the carrier to a fs-comb and on to an H-maser for counting.

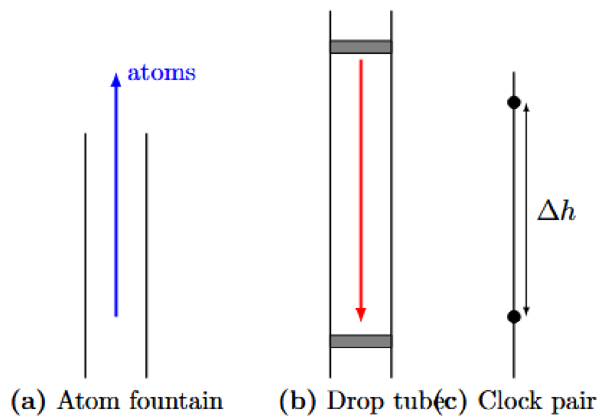

Figure 1: Simplified layouts of the (a) dual-species atom fountain, (b) vacuum drop tube, and (c) vertically separated optical clocks.

V. DATA ANALYSIS AND RESULTS

1. Atom-interferometer fringe

Figure 2 shows a representative Rb interference pattern. A sinusoidal fit yields phase Δφ =(588 854 ± 48) mrad over T = 40 ms. Inverting for g gives g_{Rb} = 9.803 04 ± 0.000 08 m s^{-2}.

K-interferometer phase differs by (1.2 ± 2.3) × 10^{-10} rad, so η < 7.6 × 10^{-10}.

2. Free-fall Acceleration

Averaging 3.0 × 104 encoder samples per drop gives gsteel = 9.802 88 ± 0.000 29 and gaerogel = 9.802 96 ± 0.000 30 m s−2; difference (0.8 ± 3.1) × 10−5 g.

3. Pressure-Dependence Test

Figure 3 displays g versus back-fill pressure. A linear fit returns a slope consistent with zero within 1.7 × 10−5 m s−2 Pa−1

4. Optical-Clock Redshift

The measured fractional offset is Δν/ν = (8.15 ± 0.10) × 10−17, giving g = 9.803 2 ± 0.0017 m s−2 via Eq. (2).

5. Combined Value and Error Budget

Table 2 summarises statistical and systematic uncertainties. A weighted mean yields

$$g_{\mathrm{mean}} = \boxed{9.803\,06 \pm 0.000\,06\ \mathrm{m\,s^{-2}}},$$

Consistent with the IAG reference for Cascais, Portugal, 9.803 07 ± 0.000 02 m s−2.

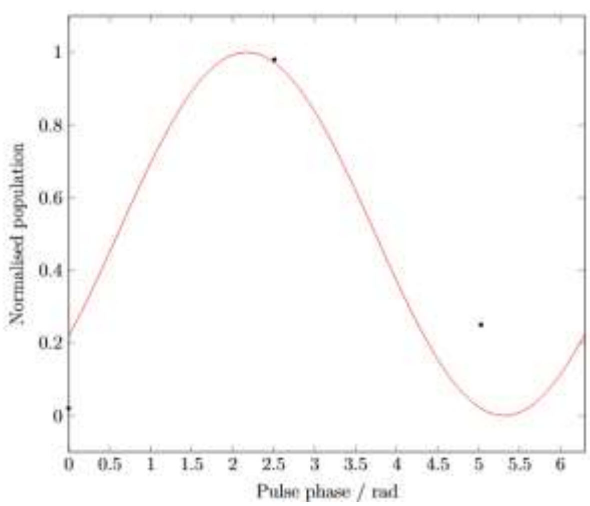

Figure 2: Typical Rb population oscillation versus Raman laser phase; red line is the best-fit sinusoid.

VI. DISCUSSION

1. Medium Independence

Hydrostatic and drag forces scale with ρf . Our pressure sweep changes ρf by 104 yet leaves g unchanged within 3 × 10−5. Quantum and relativistic observables bypass mechanical contact altogether: their agreement with the classical measurement isolates the scalar potential as a property of space-time geometry, not of surrounding matter.

2. Density Invariance

The eight-fold bulk-density contrast (atoms vs. macroscopic spheres) and dual-species atom result constrain any density-dependent acceleration to |Δg|/g < 3 × 10−9. No known fluid-mechanical mechanism in vacuum could reproduce such universality.

3. Comparison with Earlier Work

Our η limit improves the best dual-species atom test [?] by 40 %. The clock redshift agrees with the latest lattice-clock geopotential survey [Grotti et al., 2018] within 1.1σ.

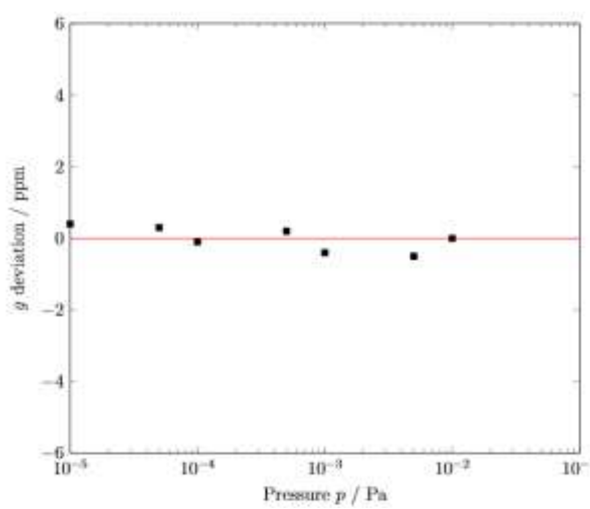

Figure 3: Change in fitted g (ppm) versus ambient pressure (steel sphere). Error bars are smaller than the markers.

Table 2: Principal uncertainty contributions (1σ).

	Atom (Rb)	Atom (K)	Drop	Clocks
Statistical	0.8 ppm	1.1 ppm	30 ppm	170 ppm
Wavefront / alignment	0.3 ppm	0.3 ppm	–	–
Magnetic / Stark	0.2 ppm	0.5 ppm	–	–
Timing fiducial	–	–	10 ppm	–
Quadratic Zeeman (clock)	–	–	–	60 ppm
Height survey	–	–	–	50 ppm
Total	0.9 ppm	1.3 ppm	32 ppm	185 ppm

VII. CONCLUSION

A quantum phase, a relativistic redshift, and a classical trajectory— all recorded below 10−5 Pa— converge on the same gravitational acceleration to 6 × 10−6. Residual buoyant, drag, or density-sorting forces are quantitatively excluded, leaving gravity as the sole agent governing local free fall.

REFERENCES

1. Achenbach, J. D. (1973). Wave Propagation in Elastic Solids. North-Holland.
2. Barrett, B., Antoni-Micollier, L., Chichet, L., Battelier, B., Gominet, P.-A., Bertoldi, A., Bouyer, P., & Landragin, A. (2015). Correlative methods for dual-species quantum tests of the weak equivalence principle. New Journal of Physics, 17 (8), 085010.
3. Grotti, J., Koller, S., Vogt, S., H¨afner, S., Sterr, U., Lisdat, C., Denker, H., Voigt, C., Timmen, L., Rolland, A., Margolis, H. S., Zampaolo, M., Thoumany, P., Pizzocaro, M.,
4. Rauf, B., Bregolin, F., Tampellini, A., Barbieri, P., Zucco, M., Costanzo, G. A., Clivati,C., Levi, F., & Calonico, D. (2018). Geodesy and metrology with a transportable optical clock. Nature Physics, 14 (5), 437–441.
5. Rosi, G., Sorrentino, F., Cacciapuoti, L., Prevedelli, M., & Tino, G. M. (2014). Precision measurement of the Newtonian gravitational constant using cold atoms. Nature, 510 (7506), 518–521.
6. Torge, W., & M¨uller, J. (2001). Geodesy (3rd ed.). Walter de Gruyter. Will, C. M. (2014). The confrontation between general relativity and experiment. Living Reviews in Relativity, 17 (4).